SCIENTIFIC REPORTS

OPEN

δ^{13}C-CH_4 reveals CH_4 variations over oceans from mid-latitudes to the Arctic

Received: 18 November 2014
Accepted: 05 August 2015
Published: 01 September 2015

Juan Yu[1], Zhouqing Xie[1], Liguang Sun[1], Hui Kang[1], Pengzhen He[1] & Guangxi Xing[2]

The biogeochemical cycles of CH_4 over oceans are poorly understood, especially over the Arctic Ocean. Here we report atmospheric CH_4 levels together with δ^{13}C-CH_4 from offshore China (31°N) to the central Arctic Ocean (up to 87°N) from July to September 2012. CH_4 concentrations and δ^{13}C-CH_4 displayed temporal and spatial variation ranging from 1.65 to 2.63 ppm, and from −50.34% to −44.94% (mean value: −48.55 ± 0.84%), respectively. Changes in CH_4 with latitude were linked to the decreasing input of enriched δ^{13}C and chemical oxidation by both OH and Cl radicals as indicated by variation of δ^{13}C. There were complex mixing sources outside and inside the Arctic Ocean. A keeling plot showed the dominant influence by hydrate gas in the Nordic Sea region, while the long range transport of wetland emissions were one of potentially important sources in the central Arctic Ocean. Experiments comparing sunlight and darkness indicate that microbes may also play an important role in regional variations.

Methane (CH_4) is an important long-lived greenhouse gas[1], which contributes directly and indirectly to radiative forcing that affects the climate[2]. Methane is also a significant reactive gas that plays an important role in tropospheric and stratospheric chemistry[3]. The oxidation of CH_4 by hydroxyl radicals (OHs) in the troposphere can lead to the formation of formaldehyde (CH_2O), ozone (O_3), carbon monoxide (CO), and water vapour. In conjunction with CO, CH_4 can control the amount of OH in the troposphere. It also reacts with Cl radicals in the stratosphere, preventing them from reducing O_3. CH_4 leves have more than doubled since the industrial revolution and the global average concentration was estimated as 1.808 ppm in 2012[4]. This increase is attributed to an excess of sources, both natural and anthropogenic, compared to sinks. Most parts of the ocean are supersaturated in CH_4 in relation to its partial pressure in the atmosphere[3]. Oceans cover roughly 70% of the earth's surface, play a critical role in controlling global temperature, and serve as a source or a sink for many atmospheric trace gases[5]. Because of the isotopic fractionation effect, CH_4 from different sources have different isotopic characteristics. The most commonly measured isotope of CH_4 is ^{13}C. Depleted-δ^{13}C is derived from bacterial sources and enriched-δ^{13}C is derived from non-bacterial sources such as natural gas and biomass burning[6]. Isotopic determination of δ^{13}C-CH_4 in the atmosphere, in conjunction with measurements of concentrations, provides a better understanding of CH_4 sources and sinks.

Ehhalt first determined a budget of sources and sinks of CH_4 related to the total atmospheric burden[7]. Since then, extensive CH_4 concentration and δ^{13}C-CH_4 measurements have been performed at sites in the Northern and Southern hemispheres[8–10]. These have provided information on the seasonal cycling of CH_4 and δ^{13}C-CH_4, sources and sinks, and long-term trends[9,11]. However, the observations have been land-based measurements that are subject to local contamination error. Contamination risk is reduced over ocean surfaces. The earliest measurements of atmospheric CH_4 over the North Atlantic and the Pacific oceans showed a weak decrease beginning at 30°N and extending to 20°S[12]. In contrast, the distribution of CH_4 determined by shipboard air-grab sampling in the South Atlantic region did not reveal clear latitudinal trends[13]. Another study on atmospheric δ^{13}C-CH_4 measurements investigated the

[1]Institute of Polar Environment, School of Earth and Space Sciences, University of Science and Technology of China, Hefei, Anhui, 230026. [2]Institute of Soil Science, Chinese Academy of Sciences, Nanjing, 210008. Correspondence and requests for materials should be addressed to Z.Q.X. (email: zqxie@ustc.edu.cn)

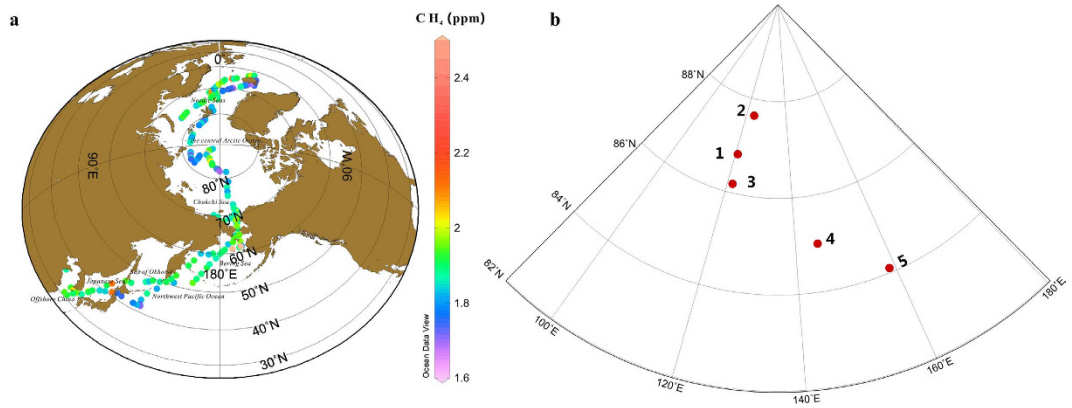

Figure 1. (**a**) Spatial distribution of atmospheric CH_4 (ppm). (**b**) Experimental sites for CH_4 flux measurements at the short-term ice stations during CHINARE 2012. Base map is from Ocean Data View (v. 4.0, Reiner Schlitzer. Alfred Wegener Institute for Polar and Marine Research, Bremerhaven, Germany).

Pacific Ocean and revealed three distinct latitudinal bands of $\delta^{13}C\text{-}CH_4$[14]. The latitudinal variations of CH_4 and $\delta^{13}C\text{-}CH_4$ are important for understanding the chemical and dynamic processes that control their distributions. Although there were reports on CH_4 distributions from 85°N to 67°S , the sources and influencing factors are still poorly understood, especially in the Arctic region[15]. Since 2007, the CH_4 concentrations had stabilized but increased again[16,17]. Systematic observations of CH_4 and $\delta^{13}C\text{-}CH_4$ over oceans remain limited. The present knowledge of atmospheric CH_4 is insufficient for describing all the variations affected by regional influencing. At high latitudes, methane is supersaturated in the surface waters of the Arctic Ocean[18,19] and European coastal areas[20]. Spatial and temporal observation of CH_4 is essential to identify and quantify the CH_4 sources. However, the direct atmospheric CH_4 concentration data and $\delta^{13}C\text{-}CH_4$ measurements are meagre over oceans from the mid- to high latitudes of the North Hemisphere, especially over the Arctic Ocean where the physical and chemical characteristics of the oceans waters have changed in response to climatic warming.

In this study, we describe new shipboard determinations of atmospheric CH_4 concentrations and $\delta^{13}C\text{-}CH_4$ measurements conducted from offshore China to the central Arctic Ocean, covering the latitudes and longitudes of 31.1°N–87.4°N and 22.8°W–90°E–166.4°W, during the 5th Chinese National Arctic Research Expedition (CHINARE 2012). This study is the first to report the temporal and spatial distributions of atmospheric CH_4 concentrations, combined with $\delta^{13}C\text{-}CH_4$ measurements, over an extensive spatial scale. The $\delta^{13}C\text{-}CH_4$ measurements revealed factors that affect CH_4 variation.

Results

Trends of atmospheric CH_4 concentrations and $\delta^{13}C\text{-}CH_4$. The spatial and latitudinal distributions of CH_4 concentrations determined during CHINARE 2012 are shown in Figs 1a and 2a, respectively. The CH_4 concentrations varied between 1.65 and 2.63 ppm. By the statistic analysis approximately 79% of the data ranged from 1.80ppm to 2.00ppm, with a median concentration of 1.88 ppm (mean: 1.88 ± 0.12 ppm), indicating that local episode influences were minimal (Fig. 2b). Based on evaluation using the Kolmogorov–Smirnov test, the CH_4 concentrations were revealed to be distributed inhomogeneously along the cruise track ($p < 0.05$), even when the four highest values were excluded. The distribution of CH_4 concentrations showed no obvious relationship with latitude outside the Arctic Ocean, which was consistent with observations from the South Atlantic[13]. However, the CH_4 concentrations in the Arctic Ocean (>66.5°N) fluctuated in a more consistent manner, especially in the central Arctic Ocean (>80°N), where concentrations increased with latitude ($r = 0.44$, $p < 0.01$).

Atmospheric $\delta^{13}C\text{-}CH_4$ varied from −50.34% to −44.94% with a median value of −48.63% (meane: $-48.55 \pm 0.84\%$) (Fig. 2c). The mean value was lower than the mean $\delta^{13}C\text{-}CH_4$ (−47.44%) reported for the northern hemisphere[9]. The higher frequencies ranged from −49.5% to −48% (Fig. 2d). A Kolmogorov–Smirnov test indicated heterogeneous distribution of $\delta^{13}C\text{-}CH_4$ along the cruise track ($p < 0.05$). From mid- to high latitudes, the $\delta^{13}C\text{-}CH_4$ measurements showed a slight decreasing trend with latitude ($r = -0.23$, $p < 0.01$). A similar decreasing trend with northern latitude was also observed between 65°S and 50°N[9] during the Pacific Ocean cruise.

Regional variations of atmospheric CH_4 concentrations and $\delta^{13}C\text{-}CH_4$. Atmospheric CH_4 and $\delta^{13}C\text{-}CH_4$ samples from the entire cruise were separated into eight groups based on geographical locations and ice-coverage characteristics: Offshore China (OC), Japanese Sea (JS), Sea of Okhotsk (SO), Northwest Pacific Ocean (NPO), Bering Sea (BS), Chukchi Sea (CS), central Arctic Ocean (CAO), and Nordic Seas (NS) (Table 1). For the sample regions outside the Arctic Ocean, the mean (±SD) CH_4 leves in the OC, JS, SO and BS areas were 1.90 ± 0.05 ppm, 2.00 ± 0.21 ppm, 1.90 ± 0.05 ppm and

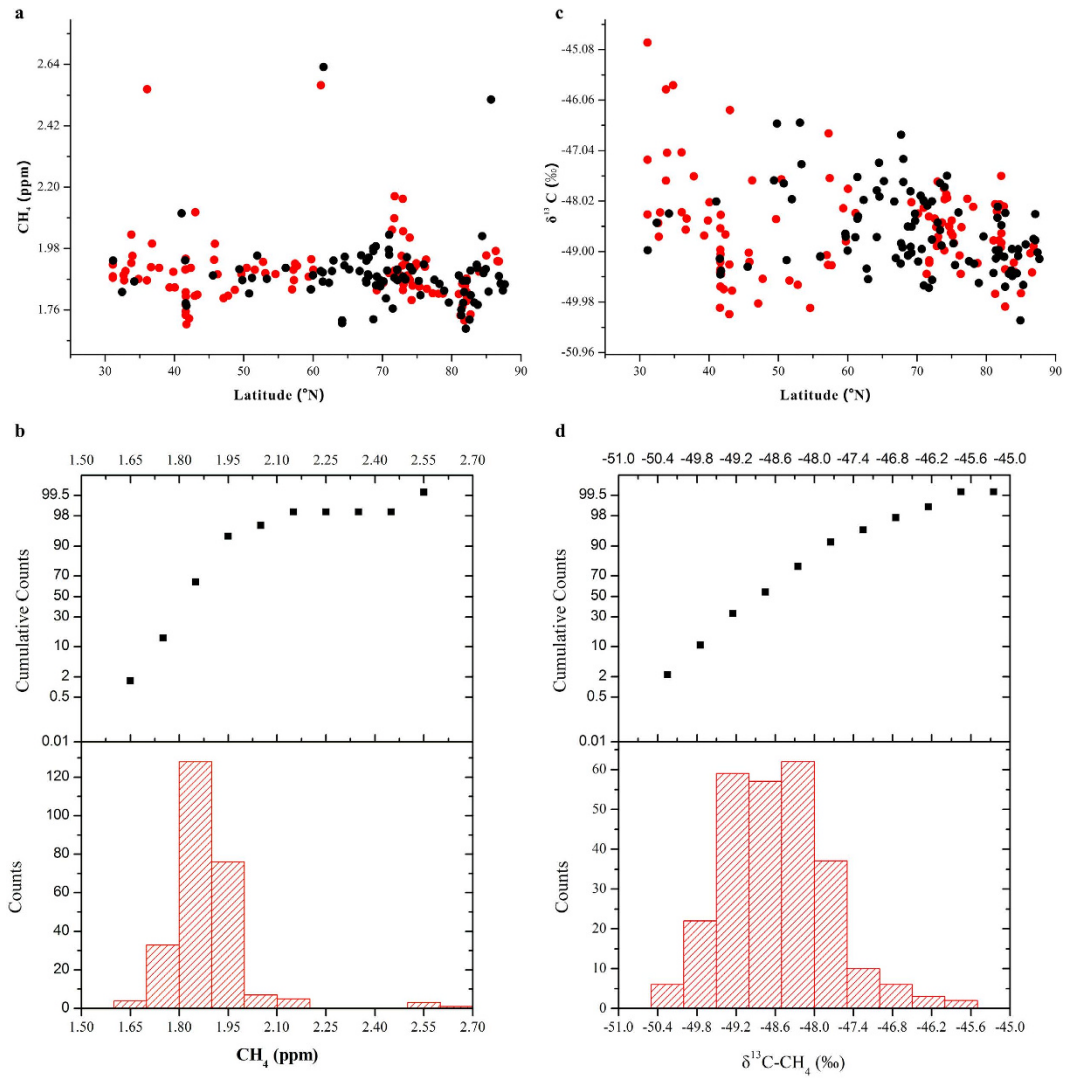

Figure 2. (**a**) Latitudinal distributions of atmospheric CH_4 during CHINARE 2012; (**b**) The frequency distribution of atmospheric CH_4; (**c**) Latitudinal distributions of $\delta^{13}C$-CH_4 during CHINARE 2012; (**d**) The frequency distribution of $\delta^{13}C$-CH_4. Red colour and black colour refer to samples collected at day and night, respectively.

Sampling Area		CH_4 (ppm)			$\delta^{13}c$-CH_4 (%)				
		Min	Max	Median	Mean ± SD	Min	Max	Median	Mean ± SD
Outside the Arctic Ocean	OC	1.82	2.03	1.89	1.90 ± 0.05	−48.97	−44.94	−47.93	−47.49 ± 1.24
	JS	1.84	2.55	1.91	2.00 ± 0.21	−48.69	−46.25	−48.29	−48.10 ± 0.70
	SO	1.83	2.00	1.89	1.90 ± 0.05	−49.20	−46.52	−48.16	−48.07 ± 0.92
	NPO	1.71	1.95	1.82	1.84 ± 0.07	−50.22	−46.50	−49.37	−49.06 ± 0.92
	BS	1.80	2.63	1.89	1.93 ± 0.17	−50.10	−46.68	−48.49	−48.50 ± 0.85
In the Arctic Ocean	CS	1.81	2.03	1.87	1.89 ± 0.05	−49.97	−46.01	−49.03	−48.78 ± 0.90
	CAO	1.69	2.51	1.85	1.86 ± 0.13	−50.34	−47.53	−48.96	−48.93 ± 0.59
	NS	1.65	2.17	1.87	1.87 ± 0.10	−49.44	−46.82	−48.31	−48.30 ± 0.54
Whole Cruise		1.65	2.63	1.88	1.88 ± 0.12	−50.34	−44.94	−48.63	−48.55 ± 0.84

Table 1. Summary of atmospheric CH4 and $\delta^{13}C$-CH_4 along the cruise during CHINARE 2012.

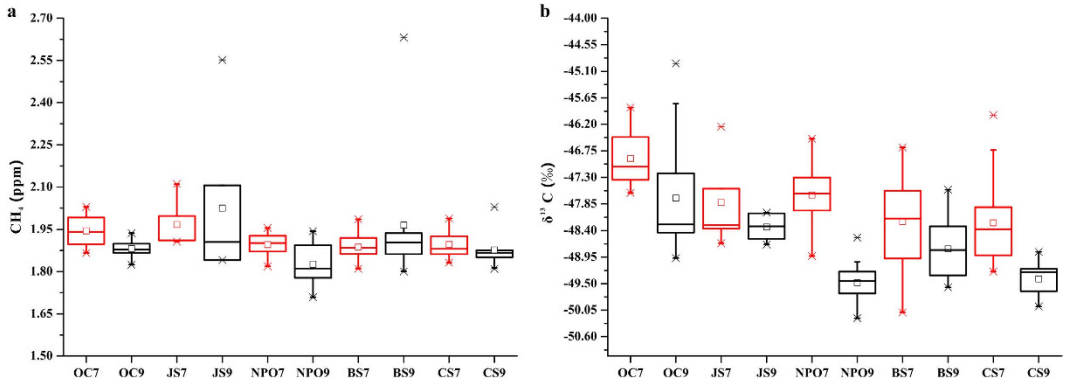

Figure 3. (**a**) Box plots of atmospheric CH_4 and (**b**) δ^{13}C-CH_4 between July (marked by red colour) and September (marked by black colour) over the OC, JS, NPO, BS, and CS regions (i.e., OC7 and OC9, JS7 and JS9, NPO7 and NPO9, BS7 and BS9, and CS7 and CS9, respectively). The lower and upper boundaries of the boxes represent the 25th and 75th percentiles, respectively. The lines and squares within or outside of the boxes mark the median and mean values, respectively. The upper and lower asterisks signify the maximum and minimum values.

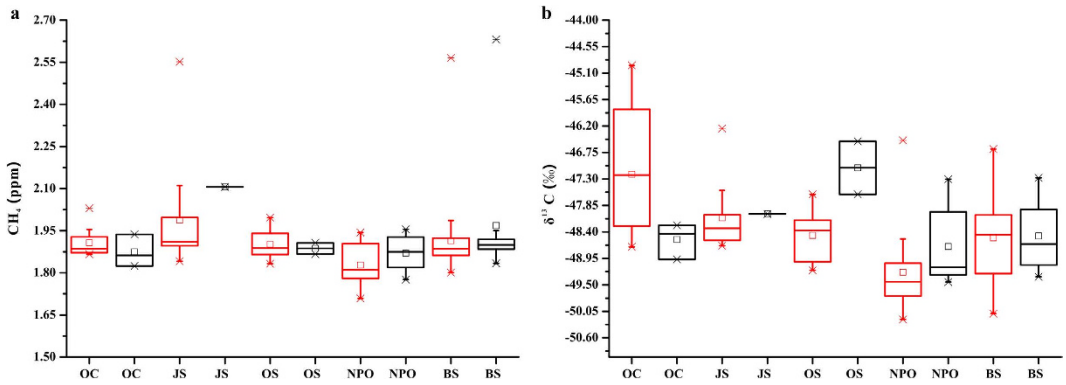

Figure 4. (**a**) Box plots of atmospheric CH_4 and (**b**) δ^{13}C-CH_4 at day (marked by red colour) and night (marked by black colour) over the OC, JS, NPO, BS, and CS regions. The lower and upper boundaries of the boxes represent the 25th and 75th percentiles, respectively. The lines and squares within or outside of the boxes mark the median and average values, respectively. The upper and lower asterisks signify the maximum and minimum values.

1.93 ± 0.17 ppm, respectively. By use of non-parametric tests, the BS and JS values were significantly higher than the CH_4 value of the NPO (1.84 ± 0.07 ppm) ($p < 0.05$). For the Arctic Ocean, the mean values of the CS, CAO, and NS areas were 1.89 ± 0.05, 1.86 ± 0.13, and 1.87 ± 0.10 ppm, respectively. Although the averages over CS, CAO, and NS were similar, some relatively higher values were found in the CAO, potentially indicating the possible presence of a CH_4 source.

The mean measurement of δ^{13}C-CH_4 in the OC region was -47.49 ± 1.24%, which was similar to the mean δ^{13}C-CH_4 (-47.44%) for the Northern Hemisphere[8]. The maximum value of δ^{13}C-CH_4 was -44.04%. However, the δ^{13}C-CH_4 values for the other regions (JS: -48.10 ± 0.70%, SO: -48.07 ± 0.92%, NPO: -49.06 ± 0.92%, BS: -48.50 ± 0.85%, CS: -48.78 ± 0.90%, CAO: -48.93 ± 0.59%, and NS: -48.30 ± 0.54%) were all lower than the mean value in the Northern Hemisphere and the closest land-based observation.

Temporal variations of atmospheric CH_4 concentrations and δ^{13}C-CH_4. The CH_4 concentrations in July and September for the same sampling regions are shown in Fig. 3a. Non-parametric tests indicated that the values in July and September were not significantly different. Figure 3b also shows no significant differences between the measurements of δ^{13}C-CH_4 in July and September in the OC, JS, and BS areas. However, the δ^{13}C-CH_4 values in NPO and CS regions were greater in July than in September.

The diurnal and nocturnal CH_4 concentrations and δ^{13}C-CH_4 measurements for the same sampling regions are shown in Fig. 4. Non-parametric tests revealed no significant differences between day and hight CH_4 concentrations and δ^{13}C-CH_4 measurements.

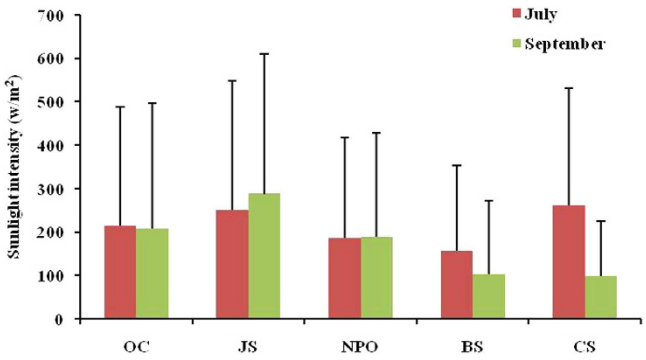

Figure 5. Variations of sunlight intensity in July and September over the OC, JS, NPO, BS, and CS regions. The error bars represent the positive standard deviation.

Discussion

Atmospheric CH_4 concentrations and $\delta^{13}C\text{-}CH_4$ over the oceans might be influenced by sources and sinks, e.g., long-range transport of anthropogenic emissions or natural sources emitted from the ocean, and by oxidation by Cl and OH radicals or microbes. Although oceanic CH_4 was not measured simultaneously in this study, environmental parameters were recorded for further analysis.

The role of oxidation. The phase of $\delta^{13}C\text{-}CH_4$ in the seasonal cycle is consistent with the kinetic isotope effect (KIE), which is due to OH and/or Cl radicals oxidizing $\delta^{12}C\text{-}CH_4$ faster than $\delta^{13}C\text{-}CH_4$, resulting in atmospheric methane enriched in $\delta^{13}C\text{-}CH_4$[9]. From mid- to high latitudes, the $\delta^{13}C\text{-}CH_4$ showed a slight decreasing trend with latitude in sunlight. The latitudinal loss of $\delta^{13}C\text{-}CH_4$ may be due to decreasing enriched input of $\delta^{13}C$ or chemical oxidation. Considering the potential fuel source influences, the variation of CO with latitude and the air masses of all the samples are shown in Figure S1. The CO concentrations showed a decreasing trend up to about 50°N, indicating a decrease in local contribution by anthropogenic sources, such as fossil fuels, north of 50°N. The back-trajectories of the air masses further confirmed the influence of continental sources of CO in the OC and JS areas (<50°N). However, the latitudinal decreasing trend of $\delta^{13}C\text{-}CH_4$ remained under background air, suggesting the potential role of oxidation. It has been reported that OH radicals in the troposphere are the primary sink for global atmospheric CH_4[21]. Cl radicals may also contribute to CH_4 loss over oceans. To determine the potential reactive process for CH_4, the contributions of the OH and Cl radicals were calculated as follows. The average concentrations of the OH and Cl radicals in the marine boundary layer are about 7×10^5–2.9×10^6 molecules·cm^{-3} and 1.8×10^4 molecules·cm^{-3}, respectively[22–25]; mean CH_4 concentration is 1.88 ppm; and the rate constant at 8 °C based on the mean sampling temperature for OH and Cl radicals is 4.42×10^{-15} and 7.59×10^{-14} cm^{-3}·molecules^{-1}·S^{-1}, respectively[26]. Assuming the reactive height is 25 m, based on the sampling height, the CH_4 consumption for OH and Cl radicals is 8.72×10^{-3}–3.61×10^{-2} mg·m^{-2}·d^{-1} and 3.85×10^{-3} mg·m^{-2}·d^{-1}, respectively. The effect of Cl radicals on CH_4 is similar to that of the OH radicals. It is unclear if the level of Cl radicals varies with latitude. However, OH radicals can decrease from low to high latitudes[23,27]. In addition, sunlight intensity at the high latitudes is lower than in the mid-latitudes. Thus, reduced oxidation in the high-latitude region might result in depleted $\delta^{13}C\text{-}CH_4$. A similar principle could explain higher values of $\delta^{13}C\text{-}CH_4$ in July compared to September over the CS area. The significantly higher sunlight intensity over the CS area in July compared with September indicated stronger oxidation potential (Fig. 5). However, the variations between July and September over the OC, JS, BS and NPO regions were not consistent with oxidation results. Most regions outside the Arctic Ocean were influenced by continental sources, and complex sources inputs may influence the oxidation results (Figure S1).

The role of sources and atmospheric transport. To determinthe potential role of sources or sinks, the variations of $\delta^{13}C\text{-}CH_4$ versus mixing ratio changes were calculated using the approach proposed by Allen *et al.* (2001)[25]. Assuming that the removal of $\delta^{13}C\text{-}CH_4$ is by OH radicals in a closed well-mixed box, the effective rate coefficient for $\delta^{12}C$ and $\delta^{13}C$ removal by OH radicals are referred to as k_{12} and k_{13}. We adopted the value $k_{13}/k_{12} = 0.9946$[28], for which $\in = k_{13}/k_{12} - 1$ is defined as the KIE. The relationship between changes in $\delta^{13}C\text{-}CH_4$ and changes in mixing ratio can be expressed as $\Delta\delta \approx \in (1 + \delta 0)\,\Delta C/C0$, which relates the $\delta^{13}C\text{-}CH_4$ variations ($\Delta\delta$) around the mean $\delta^{13}C\text{-}CH_4$ value ($\delta 0$) to relative mixing ratio variations ($\Delta C/C0$), where C0 is the mean mixing ratio over the cruise track. If we plot $\Delta\delta$ versus $\Delta C/C0$, the KIE line of slope can be obtained. The details about the expression were presented in a previous report[25]. We can also obtain the variations of $\delta^{13}C\text{-}CH_4$ and mixing ratio changes in different regions (Fig. 6a). The values over the OC, JS, SO, NS, and BS areas were above the KIE line (OH oxidation line), representing enriched $\delta^{13}C\text{-}CH_4$. Enriched $\delta^{13}C\text{-}CH_4$ may mean more oxidation by OH radicals. If the

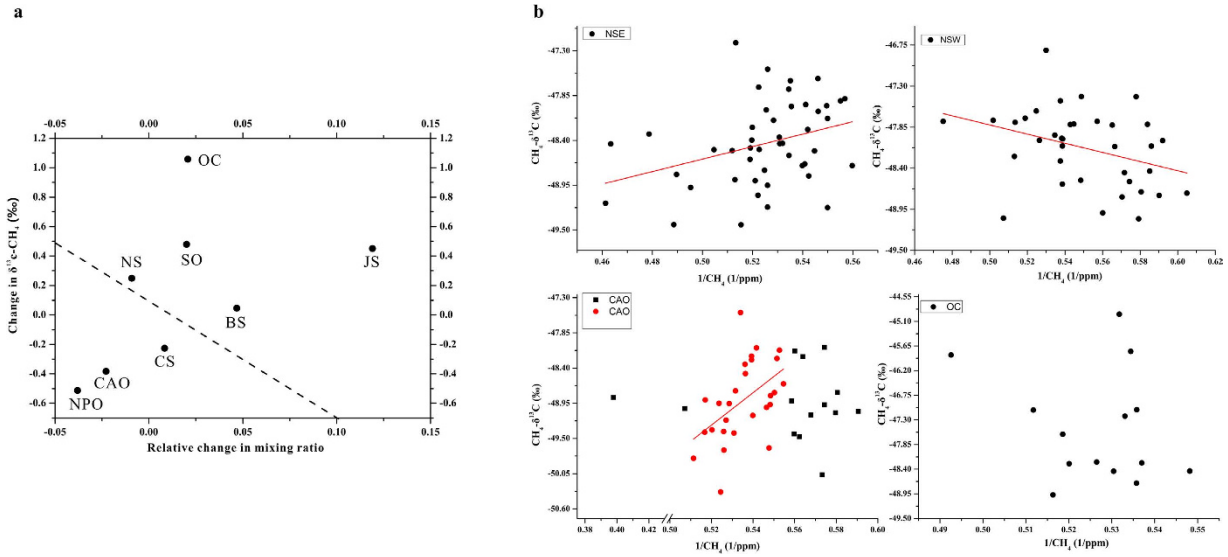

Figure 6. (**a**) Variations of CH_4 mixing ratio and $\delta^{13}C$-CH_4 in different regions. The dashed line is the KIE line. (**b**) Examples of corresponding Keeling plot over NS, CAO and OC.

enriched $\delta^{13}C$-CH_4 was influenced by other forms of oxidation such as by Cl radicals, the CH_4 concentration should be lower. The higher values signified an anthropogenic source, especially for the samples over the OC and JS regions that were far from the KIE line, suggesting that anthropogenic sources might play a major role. The values from the CAO, CS, and NPO areas were below the KIE line and the depleted $\delta^{13}C$-CH_4 might indicate a natural source or less oxidation. If the lower values over the CAO, CS, and NPO areas were a reflection of reduced oxidation only, the concentrations would be higher and thus, the low values signify natural sources.

However, this box model only provided potential sources due to it requiring knowledge of how the out of the box values changing. We therefore applied Keeling plot approach to further investigate the regional variations. If the CH_4 is emitted into the atmosphere from a single source, the isotopic ratio of the source can be inferred as an end-member for the baseline on the Keeling plot[29,30]. It was reported that biogenic sources were dominant at Spitsbergen[29]. Figure 6b shows examples of $\delta^{13}C$-CH_4 plotted against the reciprocal of CH_4 for the regions over NS and CAO regions, both of them close to Spitsbergen, and the OC region influenced by anthropogenic sources. NS was divided into east NS (NSE) close to Spitsbergen and west NS (NSW) close to Iceland, based on the geographical location. The Keeling plot can be used to understand the processes controlling isotope discrimination and to estimate the isotopic ratio of a source[31]. The CH_4 collected in NSE gave a source with -52.46% ($r = 0.33$, $p < 0.05$), which is similar to the observations at Zeppelin station during Arctic springtime[29]. The main source in the NSE was gas field emissions as few air masses over this were from known emission areas. In contrast, the $\delta^{13}C$-CH_4 of -44.75% ($r = 0.35$, $p < 0.05$) signature in NSW indicated enriched $\delta^{13}C$ inputs. Iceland is a geothermal country. Air masses close to Iceland with heavier $\delta^{13}C$ may have contributed to the increment in NSW. However, in CAO we collected CH_4 data in a scale from 1.8 to 2.0 ppm, the highest frequency range. This indicated a source with -62.45% ($r = 0.50$, $p < 0.01$) suggesting that the wetlands dominated. The isotope data was consistent with the Siberian railroad and the Ob river with -62.9%[32]. The main air masses in CAO move across the west Siberian coast, also confirming the wetlands emission (Figure S2). But there were some enriched and depleted sources inputs, indicating CAO was influenced by complex mixing sources. It has been demonstrated that extra sources may change seasonal variation[25]. One example outside the Arctic Ocean is the OC region which has complex mixing sources (Fig. 5b). Complex mixing sources may influence the results of seasonal variation outside the Arctic Ocean.

The role of microbes. The $\delta^{13}C$-CH_4 should be enriched in sunlight and depleted in darkness in the same region because of the higher photochemical oxidation rate in sunlight. However, we found no significant differences in the CH_4 concentrations and $\delta^{13}C$-CH_4 measurements between sunlight and darkness in this study. This might be due to microbes producing more CH_4, which can be deduced based on the case study of CH_4 variation in sunlight and darkness over the central Arctic Ocean. The CH_4 fluxes on sea ice in sunlight and darkness are shown in Fig. 7. CH_4 fluxes on sea ice had positive (emission) or negative (absorption) values[19]. Methanogenic bacteria and methanotrophic bacteria can occur in cold marine waters and in sea ice[33,34]. Thus, the CH_4 emissions might come from the CH_4 in the water[18] and from CH_4 production by microorganisms in the sea ice[35]. During CHINARE 2010, we suggested that negative fluxes could be associated with both photochemical and biochemical oxidation[19]. However, photochemical oxidation cannot explain why lower CH_4 fluxes were observed in the dark

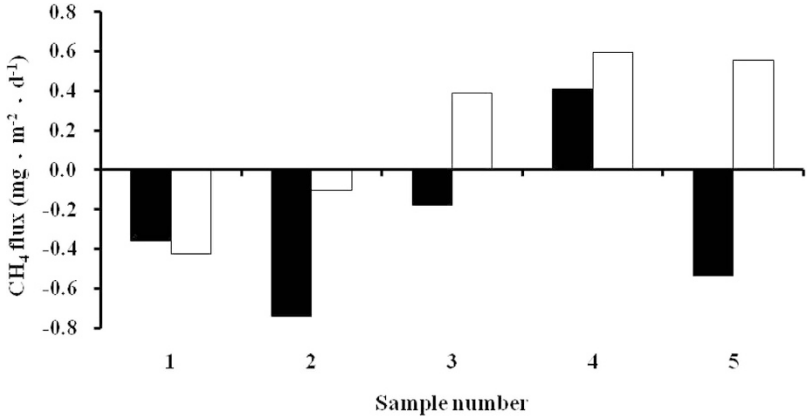

Figure 7. CH_4 fluxes at short-term ice stations under conditions of sunlight (blank) and darkness (black).

than in sunlight. The negative fluxes could be attributed to the role of methanotrophs. Llight inhibits the growth and activity of methanotrophic bacteria[36], which could result in the reduced loss of CH_4 in sunlight compared with darkness. Additionally, temperatures are higher in sunlight than in darkness and methanogenic bacteria can increase CH_4 production at higher temperature[37]. Archaeal populations of methanogenic and methanotrophic bacteria can be abundant in cold and temperate environments[37]. In temperate environments, the depleted $\delta^{13}C$-CH_4 produced by microbes in the sunlight might offset the sink of chemical oxidation.

Experimental Methods

Sampling gas. During CHINARE 2012 (July-September 2012) air samples were collected from the marine boundary layer using 17.5-ml vacuum vials (manufactured by the Institute of Japanese Agricultural Environment) and 0.5-l Tedlar gas bags to determine the CH_4 concentrations and values of $\delta^{13}C$-CH_4, respectively. The samples in the gas vacuum vials were sealed with a butyl-rubber septum and a plastic cap, following the same sampling method used in the research on Antarctica[38]. The cruise covered the eight geographical areas shown in Fig. 1a. The sampling location was the fifth deck of the icebreaker *Xuelong*, which was about 25 m above sea level. To avoid contamination by ship emissions and anthropogenic factors the samples were collected upwind. The gas vacuum vial was equilibrated in the air for about 1 min using a two-way needle above the head. Samples were collected two or three times each day. The sampling times after 06:00 and 18:00 (local time) were considered as day (sunlight) and night (darkness), respectively. Ancillary data including sunlight intensity and CO concentrations analysed using an EC9830 monitor were also recorded along the cruise track[39]. CH_4 fluxes on sea ice in sunlight and darkness (simulating day and night) were determined using a static chamber technique less than 2 h at five short-term ice stations (sites shown in Fig. 1b). The procedure was based upon a previous report[14]. The inner diameter of the cylindrical chamber was 0.4×0.3 m. The open-bottomed acrylic resin chambers were placed on collars installed at the measurement sites. The use of the collars allowed the same spot to be measured repetitively, ensures that the chamber is well sealed, and minimizes site disturbance. One chamber allowed sunlight transmission and the other did not permit sunlight. Once the chamber was set up, the head-space samples were immediately transferred into the vacuum vial using a two-way needle[19]. The sampling procedures were repeated at 20- or 30-min intervals for about 2 h at each site. All collected samples were analysed in the laboratory of the Institute of Soil Science, Chinese Academy of Sciences, Nanjing, China.

Determination of CH_4 concentrations and fluxes. An Agilent 7890 A gas chromatograph (GC) with a flame ionization detector (FID) was used to determine the CH_4 concentrations. The GC-FID was equipped with an auto-injection system controlled by a computer program and a back-flushed system of 10-port valves. The chromatographic column was a 2-m stainless steel column filled with high-performance Molecular Sieve 13X. The column and detector temperatures were 85 and 250 °C, respectively. The flow rates of N_2, H_2, and air were 25, 60, and 380 ml/min, respectively. CH_4 standard gas at 10ppm was produced by the National Institute of Metrology, China (NIMC). The GC analysis and calibration were according to GB/T 8984–2008 (NIMC). The calibration scale had a range of 0.95~49.8 ppm. The GC instrument was calibrated using CH_4 standard gas every twelve samples. The variance coefficient (CV) for each measured sample and each time was $<1\%$. CH_4 fluxes were calculated using the following equation: $P(CH_4) = \rho \cdot H \cdot \frac{dc}{dt} \cdot \frac{273}{273+t} \cdot 24$, where $P(CH_4)$ is the CH_4 flux ($mg \cdot m^{-2} \cdot d^{-1}$), ρ is the density of CH_4 gas under standard conditions ($0.714\,kg \cdot m^{-3}$), H is the height of the chamber (m), dc/dt is the time derivation of CH_4 in the chamber ($ppm \cdot h^{-1}$), and t is the average temperature (°C)in the chamber[19,40].

Determination of δ^{13}C-CH_4. The δ^{13}C-CH_4 value was measured using a Thermo Finnigan Mat-253 Isotopic Mass Spectrometer. The Mat-253 mass spectrometer has a fully automated interface for the pre-GC and pre-concentration of trace gases. Full details of the method were described by Cao[41] and a brief description is given here. In this study, 100-ml gas samples were injected into vacuum glass bottles. If the gas sample was <100 ml, inert gases without CH_4 was added to the bottle and the bottle was adjusted to normal pressure. The air-sampling bottles were installed into pre-concentration. After their thresholds were blown by He gas, the valves at either end of the sampling bottles were opened and the samples blown into the cold trap by He. At the temperature of -196 °C, only the volatile components (N_2, O_2, Ar, and CH_4) can enter the 1000 °C burning furnace via the cold trap and an aluminous oxidative pipe filled with three 0.13-mm nickel wires. During the test period, CH_4 is oxidized into CO_2 and H_2O. The CO_2 produced from the CH_4 combustion was collected by another cold trap and transported into a third cold trap. Then, CO_2 was passed into the GC for further separation. The calibrated standard CO_2 was injected into the ionic source three times continuously every 30 s. The ionic flows of m/z 44[$^{12}C^{16}O^{16}O]^+$, m/z 45[$^{13}C^{16}O^{16}O]^+$, and m/z 46[$^{12}C^{16}O^{18}O]^+$ were accepted by cup2, cup3, and cup4, respectively. Adjusting the flow rate of the reference gas controlled the peak intensity of m/z 44 to within 2v–3v. The No. 2 peak was set as the standard sample peak. The CH_4 peak occurred at about 870 s and the ratio line was positive. According to the ratios of the No. 2 CO_2 peak and the sample peak, the $\delta^{13}C_{PDB}$ for the CO_2 from the CH_4 was obtained. The 2.02 μl/l compressed CH_4 was from the same source. Then, 25 ml of compressed CH_4 was injected into a 100-ml glass bottle with an inert gas filling under normal pressure nine times. The standard deviation for δ^{13}C-CH_4 in the compressed air was 0.196% based on the nine repeated measurements. The different CH_4 concentrations showed good relationships with ionic flows of m/z 44, and the correlation coefficient was 0.983. GBW04407 (carbon black, national standard substance produced by NIMC with -23.73% for $\delta^{13}C_{VPDB}$) were used to calibrate the carbon isotope[40]. Isotope ratios were defined as $\delta^{13}C = [(R_{sample}/R_{standard}) - 1] \times 1000[\%]$, where $\delta^{13}C$ is the δ value of the carbon isotope and R is the ratio of the heavy isotope to the light isotope.

References

1. Dickinson, R. E. & Cicerone, R. J. Future global warming from atmospheric trace gases. *Nature* **319,** 109–115 (1986).
2. Forster, P. *et al. Changes in atmospheric constituents and in radiative forcing*. 135–136 (Cambridge University Press, 2007).
3. Cicerone, R. J. & Oremland, R. S. Biogeochemical aspects of atmospheric methane. *Glob. Biogeochem. Cycle* **2,** 299–327 (1988).
4. Blunden, J., Arndt, D. S. & Achberger, C. State of the Climate in 2012. *Bull. Amer. Meteor. Soc.* **94,** S1–S238 (2013).
5. Anderson, B. *et al. Methane and Nitrous Oxide Emissions From Natural Sources*. (U.S. Environmental Protection Agency, 2010).
6. Wuebbles, D. J. & Hayhoe, K. Atmospheric methane and global change. *Earth-Sci. Rev.* **57,** 177–210 (2002).
7. Ehhalt, D. The atmospheric cycle of methane. *Tellus* **26,** 58–70 (1974).
8. Dlugokencky, E. J., Steele, L. P., Lang, P. M. & Masarie, K. A. Atmospheric methane at Mauna Loa and Barrow observatories: Presentation and analysis of *in situ* measurements. *J. Geophys. Res.* **100,** 23103–23113 (1995).
9. Quay, P. *et al.* The isotopic composition of atmospheric methane. *Glob. Biogeochem. Cycle* **13,** 445–461 (1999).
10. Dlugokencky, E., Steele, L., Lang, P. & Masarie, K. The growth rate and distribution of atmospheric methane. *J. Geophys. Res.* **99,** 17021–17043 (1994).
11. Tyler, S. C., Rice, A. L. & Ajie, H. O. Stable isotope ratios in atmospheric CH_4: Implications for seasonal sources and sinks. *J. Geophys. Res.* **112,** D03303 (2007).
12. Ehhalt, D. The CH_4 concentration over the ocean and its possible variation with latitude. *Tellus* **30,** 169–176 (1978).
13. Alvala, P. C., Boian, C. & Kirchhoff, V. Measurements of CH_4 and CO during ship cruises in the South Atlantic. *Atmos. Environ.* **38,** 4583–4588 (2004).
14. Lowe, D. C. *et al.* Shipboard determinations of the distribution of ^{13}C in atmospheric methane in the Pacific. *J. Geophys. Res.* **104,** 26125–26135 (1999).
15. Wofsy, S. HIAPER Pole-to-Pole Observations (HIPPO): fine-grained, global-scale measurements of climatically important atmospheric gases and aerosols. *Phil. Trans. R. Soc. A* **369,** 2073–2086 (2011).
16. Dlugokencky, E. *et al.* Observational constraints on recent increases in the atmospheric CH4 burden. *Geophys. Res. Lett.* **36,** L18803 (2009).
17. Nisbet, E. G., Dlugokencky, E. J. & Bousquet, P. Methane on the rise—again. *Science* **343,** 493–495 (2014).
18. Kort, E. *et al.* Atmospheric observations of Arctic Ocean methane emissions up to 82° north. *Nat. Geosci.* **5,** 318–321 (2012).
19. He, X. *et al.* Sea ice in the Arctic Ocean: Role of shielding and consumption of methane. *Atmos. Environ.* **67,** 8–13 (2013).
20. Bange, H. W. Nitrous oxide and methane in European coastal waters. *Estuar. Coast. Shelf Sci.* **70,** 361–374 (2006).
21. Kirschke, S. *et al.* Three decades of global methane sources and sinks. *Nat. Geosci.* **6,** 813–823 (2013).
22. Cooper, D. J. Estimation of hydroxyl radical concentrations in the marine atmospheric boundary layer using a reactive atmospheric tracer. *J. Atmos. Chem.* **25,** 97–113 (1996).
23. Bahm, K. & Khalil, M. A new model of tropospheric hydroxyl radical concentrations. *Chemosphere* **54,** 143–166 (2004).
24. Allan, W., Struthers, H. & Lowe, D. Methane carbon isotope effects caused by atomic chlorine in the marine boundary layer: Global model results compared with Southern Hemisphere measurements. *J. Geophys. Res.* **112,** D04306 (2007).
25. Allan, W., Manning, M., Lassey, K., Lowe, D. & Gomez, A. Modeling the variation of $\delta^{13}C$ in atmospheric methane: Phase ellipses and the kinetic isotope effect. *Glob. Biogeochem. Cycle* **15,** 467–481 (2001).
26. Sander, S. *et al.* Chemical Kinetics and Photochemical Data for Use in Atmospheric Studies (NASA,Jet Propulsion Laboratory,California Institute of Technology Pasadena,California, 2006).
27. Naik, V. *et al.* Preindustrial to present-day changes in tropospheric hydroxyl radical and methane lifetime from the Atmospheric Chemistry and Climate Model Intercomparison Project (ACCMIP). *Atmos. Chem. Phys.* **13,** 5277–5298 (2013).
28. Cantrell, C. A. *et al.* Carbon kinetic isotope effect in the oxidation of methane by the hydroxyl radical. *J. Geophys. Res.* **95,** 22455–22462 (1990).
29. Fisher, R. E. *et al.* Arctic methane sources: Isotopic evidence for atmospheric inputs. *Geophys. Res. Lett.* **38** (2011).
30. Dlugokencky, E. J., Nisbet, E. G., Fisher, R. & Lowry, D. Global atmospheric methane: budget, changes and dangers. *Phil. Trans. R. Soc. A* **369,** 2058–2072 (2011).
31. Pataki, D. *et al.* The application and interpretation of Keeling plots in terrestrial carbon cycle research. *Glob. Biogeochem. Cycle* **17** (2003).

32. Tarasova, O. *et al.* Atmospheric CH 4 along the Trans-Siberian railroad (TROICA) and river Ob: Source identification using stable isotope analysis. *Atmos. Environ.* **40,** 5617–5628 (2006).
33. Cavicchioli, R. Cold-adapted archaea. *Nat. Rev. Microbiol.* **4,** 331–343 (2006).
34. Trotsenko, Y. A. & Khmelenina, V. N. Aerobic methanotrophic bacteria of cold ecosystems. *FEMS Microbiol. Ecol.* **53,** 15–26 (2005).
35. Rohde, R. A. & Price, P. B. Diffusion-controlled metabolism for long-term survival of single isolated microorganisms trapped within ice crystals. *Proc. Natl. Acad. Sci. USA* **104,** 16592–16597 (2007).
36. Dumestre, J. *et al.* Influence of Light Intensity on Methanotrophic Bacterial Activity in Petit Saut Reservoir, French Guiana. *Appl. Environ. Microbiol.* **65,** 534–539 (1999).
37. Hoj, L., Olsen, R. A. & Torsvik, V. L. Effects of temperature on the diversity and community structure of known methanogenic groups and other archaea in high Arctic peat. *ISME J.* **2,** 37–48 (2008).
38. Liu, Y., Zhu, R., Li, X., Xu, H. & Sun, L. Temporal and spatial variations of atmospheric methane concentration and δ^{13}C-CH_4 near the surface on the Millor Peninsula, East Antarctica. *Chinese Journal of Polar Science* **20,** 22–31 (2009).
39. Yu, J. *et al.* High variability of atmospheric mercury in the summertime boundary layer through the central Arctic Ocean. *Sci. Rep*. **4,** 6091 (2014).
40. Zhu, R. & Sun, L. Methane fluxes from tundra soils and snowpack in the maritime Antarctic. *Chemosphere* **59,** 1583–1593 (2005).
41. Cao, Y., Sun, G., Han, Y., Sun, D. & Wang, X. Determination of nitrogen, carbon and oxygen stable isotope retios in N_2O, CH_4 and CO_2 at natural abundance levels. *Acta Pedologica Sinica* **45,** 249–258 (2008).

Acknowledgments

This research was supported by grants from the National Natural Science Foundation of China (Project Nos. 41025020, 41176170), the Program of China Polar Environment Investigation and Assessment (Project No. CHINARE2011–2015) and the Fundamental Research Funds for the Central Universities. The authors acknowledge the NOAA Air Resources Laboratory (ARL) for making the HYSPLIT transport and dispersion model available on the Internet (http://www.arl.noaa.gov/ready.html).

Author Contributions

Z.Q.X. and L.G. Sun initialed the study. Z.Q.X. designed and supervised the study. J.Y. and H.K. performed the experiment. J.Y. and Z.Q.X. wrote the manuscript. G.X.X. contributed to the samples preparation and analysis. L.G.S. and P.Z.H. contributed to the discussion of results.

Additional Information

Supplementary information accompanies this paper at http://www.nature.com/srep

Competing financial interests: The authors declare no competing financial interests.

How to cite this article: Yu, J. *et al.* δ^{13}C-CH_4 reveals CH_4 variations over oceans from mid-latitudes to the Arctic. *Sci. Rep.* **5**, 13760; doi: 10.1038/srep13760 (2015).